Bioconjugate Chemistry

Article

pubs.acs.org/bc

Inflammation Targeted Gd^{3+}-Based MRI Contrast Agents Imaging Tumor and Rheumatoid Arthritis Models

Arthur Ho-Hon Leung,[‡] Jiefu Jin,[‡] Shuxia Wang,[§] Hao Lei,[§] and Wing-Tak Wong*[,†,#,⊥]

[†]Department of Applied Biology and Chemical Technology, The Hong Kong Polytechnic University, Hung Hom, Kowloon, Hong Kong, China

[‡]Department of Chemistry, The University of Hong Kong, Pokfulam, Hong Kong, China

[§]Wuhan Center for Magnetic Resonance, State Key Laboratory of Magnetic Resonance and Atomic and Molecular Physics, Wuhan Institute of Physics & Mathematics, Chinese Academy of Sciences, Wuhan 430071, Hubei China

[#]PearL Materia Medica Development (Shenzhen) Ltd., Shenzhen 518057, China

[⊥]Henry Cheng Research Laboratory for Drug Development, The Hong Kong Polytechnic University, Hung Hom, Kowloon, Hong Kong, China

Supporting Information

ABSTRACT: Inflammatory responses are closely related to cancer progression and several diseases. Anti-inflammatory drugs that bind to inducible enzymes can be used as biomarkers for molecular imaging. Selective targeted contrast agents are expected to improve contrast-to-noise ratio (CNR) in MRI at the site of inflammation. In this work, three new Gd^{3+} DO3A-amide MRI contrast agents (CAs) that conjugated to mefenamic acid (MA), a commonly used nonsteroidal anti-inflammatory drug (NSAID), through different linkers, ethylenediamine (GdL1), 2,2′-oxidiethylamine (GdL2) and 4,7,10-trioxa-1,13-tridecanediamine (GdL3) were studied. Their relaxivities were GdL1 (4.74 mM^{-1} s^{-1}), GdL2 (4.77 mM^{-1} s^{-1}), and GdL3 (4.95 mM^{-1} s^{-1}) at 400 MHz at 25 °C. Their serum albumin binding properties were studied by tryptophan emission-quenching experiments, with GdL1 showing a preferential binding toward HSA and BSA as compared with GdL2 and GdL3. They showed low cytotoxicities toward HeLa cells at high concentration (0.5 mM) and high cellular uptake in U87 cells as compared with GdDOTA. *In vivo* MRI showed increased T1-weighted contrast after intravenous injection of the agents. Moreover, T1 contrast was significantly enhanced for 1.5 h in the U87 tumor model and 2 h in the arthritis joint in adjuvant-induced arthritis (AIA) model at dosages of 0.1 and 0.03 mmol/kg, respectively. Most of the agents were cleared at 24 h post-administration in the AIA model with no observable T1 contrast. GdL1−3 showed superior retentions and intensity enhancements (IEs) at the kidney, liver, tumor, and arthritis joint to those of GdDOTA. GdL3 showed the highest relaxivity and IE at the arthritis joint and is therefore a potential candidate to be developed as MRI CAs that target inflammation.

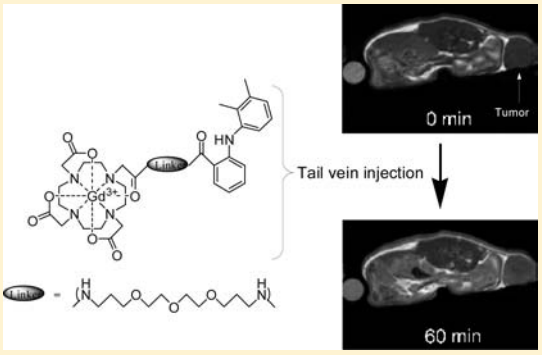

INTRODUCTION

Inflammation is an adaptive response that occurs in the early stages of several diseases that involve the production of various inflammatory mediators. Targeting these mediators based on the anti-inflammatory effect of nonsteroidal anti-inflammatory drugs (NSAIDs) can be a promising approach to target the site of inflammation.[1,2]

NSAIDs are the most common medications for the treatment of analgesic, antipyretic, and anti-inflammatory actions worldwide. They have been shown to reduce the risk of colon cancer.[3] Meanwhile, there are more findings that show the involvement of inflammation in the early stages of malignancies. They also treat rheumatoid arthritis (RA) which is known to be a chronic inflammatory disease that may cause irreversible joint damage.[4] It is generally accepted that NSAIDs have the therapeutic effects of inhibiting cyclooxygenase (COX), as established by Vane and co-workers in 1971.[5−7] Although there is evidence suggesting that NSAIDs may modulate the COX-independent signal transduction pathways,[8−10] their anti-inflammatory actions at physiologically relevant concentrations rest primarily on their inhibition of COX which consists of two isoforms, COX-1 and COX-2.[11,12] COX-1 is found to be distributed almost ubiquitously in most tissues and appears to be responsible for the production of prostaglandins (PGs) that control normal physiological functions such as regulation of renal blood flow and maintenance of the gastric mucosa. COX-2 is the inducible form of the enzyme that produces PGs in neoplastic and

Received: March 27, 2014
Revised: May 22, 2014
Published: May 23, 2014

   dx.doi.org/10.1021/bc5001356 | Bioconjugate Chem. 2014, 25, 1112−1123

Scheme 1. Synthetic Procedures of GdL1, GdL2, and GdL3[a]

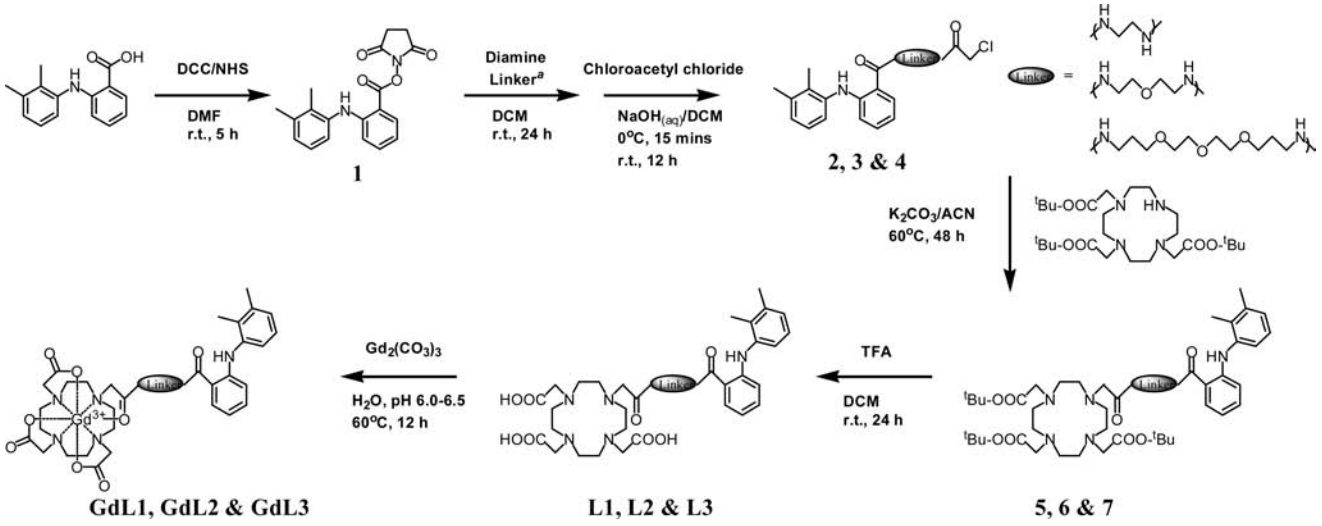

[a]Diamine linkers used in the synthesis of (2), (3), and (4) are ethylenediamine, 2,2′-oxidiethylamine, and 4,7,10-trioxa-1,13-tridecanediamine, respectively.

inflamed tissues and has been implicated in the growth and progression of human cancers such as colon, breast, ovarian, glioma, lung, and prostate cancers.[13]

There are several approaches that target inflammatory mediators for the imaging of inflammation. Muller and co-workers have reported an MRI CA that consists two sialyl Lewis^x (sLex)A moieties linked with gadolinium-diethylene-triaminepentaacetic acid (GdDTPA).[14] This probe showed an affinity toward E-selectin which is expressed on the inflamed vascular endothelial cells in hepatitis liver. It demonstrated higher and prolonged liver signal intensities in a hepatitis mouse than those in a healthy mouse. Recently, Marnett and co-workers have reported a fluorinated derivative of celecoxib, a COX-2 selective NSAID that targets COX-2 at inflammation sites by in vivo positron electron tomography (PET) imaging.[15] The selectivity was shown by the selective accumulation of this agent in the human head and neck squamous cell carcinoma (1483) xenograft that expresses COX-2. These examples have demonstrated the success of in vivo targeting on inflammation.

Magnetic resonance imaging (MRI) offers advantages such as the lack of ionizing radiation and excellent three-dimensional imaging of soft tissues. It is capable of primary tumor assessment and the determination of synovitis in patients with early rheumatoid arthritis (RA).[16,17] Their excellent spatial resolution in soft tissue provides valuable information on diseases such as Alzheimer's disease,[18] Parkinson's disease,[19] cardiovascular disease,[20] diabetes,[21] and rheumatism.[22] However, clinically approved Gd^{3+}-based MRI CAs are typically small molecular weight complexes with a hydrophilic chelating ligand that distribute nonspecifically (such as GdDTPA and GdDOTA) or at the liver (such as GdBOPTA) after administration. There is a need for a specific and effective CA that highlights diseased tissues in diagnostic medical imaging.

The present study aims to investigate the potential MRI efficiency of Gd^{3+} contrast agents bearing a mefenamic acid (MA) moiety toward the site of inflammation. MA is a NSAID that bears a dimethylphenyl group responsible for the moderate COX-2 selective ratio against COX-1 in blood ($IC_{50,COX-1}/IC_{50,COX-2}$ = 0.08, inhibition to COX-2 is 12.5-fold higher than that to COX-1)[23] and acts as a reversible human serum albumin (HSA) binding group to give a long retention time in the blood.[24] Moreover, MA is effectively excreted through both the kidney and the liver.[25] Incorporation of MA to MRI CAs may provide the following excellent properties: (i) COX-2 selectivity gives a greater retention difference between inflamed tissues and healthy tissues; (ii) the long blood retention time allows significant uptake at the site of interest; (iii) the significant renal and hepatic excretions allow imaging on both the kidney and the liver; and (iv) MA as a clinically approved NSAID has shown low toxicity toward humans. In this study, we have investigated Gd complexes which incorporated MA to thermodynamically and kinetically stable macrocycle (DOTA). The low water solubility of MA is overcome by inserting MA to a water-soluble poly(ethyleneoxy) (PEO) linker. In addition, the PEO group has been found to contribute to the biodistribution[26,27] and relaxometric properties[28,29] of Gd^{3+} complexes. Three Gd^{3+} DO3A-amide (GdL1−3) complexes were coordinated to MA through three different linkers, ethylenediamine, 2,2′-oxidiethylamine, and 4,7,10-trioxa-1,13-tridecanediamine, which differ in the degree of hydrophilicity and chain length. Their relaxivities, serum albumin binding abilities, cytotoxicities, and cellular uptake properties were studied and compared with those of gadolinium-1,4,7,10-tetraazacyclododecane tetraacetic acid (GdDOTA). Two animal models, (i) U87 xenograft, where U87 cell line has a low COX-1 level and an overexpressed COX-2 level which have been demonstrated by Western blot analysis,[30,31] and (ii) adjuvant induced arthritis (AIA) model, where COX-2 was readily detected in synovial tissues of patients with RA,[32] were used to evaluate MRI properties. These complexes demonstrate the first example that utilizes NSAID as a potential inflammation targeting moiety in MRI.

RESULTS AND DISCUSSION

Synthesis of GdL1−3. GdL1, GdL2, and GdL3 were prepared according to Scheme 1. One was prepared by the activation of *N*,*N*′-dicyclohexylcarbodiimide (DCC) coupling and then underwent nucleophilic attack by *N*-hydroxysuccinimide (NHS) in DMF. The freshly prepared 1 was purified by

dx.doi.org/10.1021/bc5001356 | Bioconjugate Chem. 2014, 25, 1112−1123

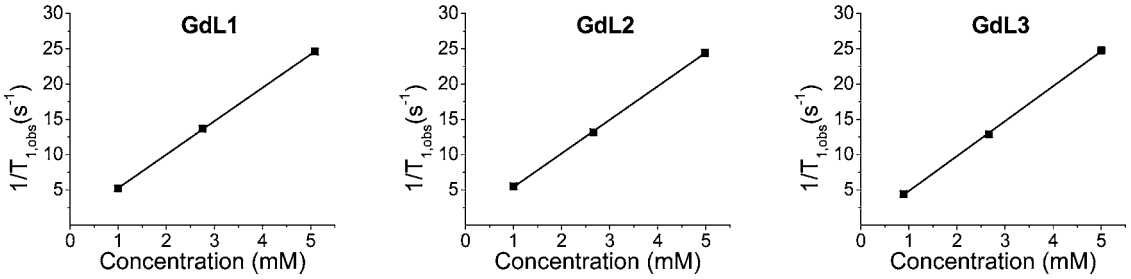

Figure 1. Plots of the $1/T_{1,\,obs}$ (r1) versus the concentration of the contrast agents GdL1, GdL2, and GdL3 at 400 MHz.

flash column chromatography on silica using $CHCl_3$ as the eluate and then added dropwise into the corresponding excess diamine solutions to give the monosubstituted amine intermediates. The excess diamine was washed away by brine. 2−4 were then prepared by condensing excess chloroacetyl chloride with the monosubstituted intermediates in DCM using aqueous NaOH as base. The resultant 2−4 were purified by extraction with brine and column chromatography on silica using $CHCl_3$ as the eluate. Tri-*tert*-butyl-1,4,7,10-tetraazacyclododecane-1,4,7-triacetate (tricyc) was prepared by coupling 1,4,7,10-tetraazacyclododecane and *tert*-butyl bromoacetate in acetonitrile using sodium hydrogen carbonate as base.[33] The tricyc and 2−4 were coupled together in dry acetonitrile using K_2CO_3 as base. The resultant 5−7 were purified by column chromatography on silica (eluent gradient from $CHCl_3$ to $CHCl_3$/MeOH, 9.5:0.5). The formation of the products was indicated by the presence of fragment peaks $[M - n \times 56]^+$ (n = 1−3) m/z in electrospray ionization mass spectrometry (ESI-MS) spectra which represented the cleavage of the three *tert*-butyl groups. The purity of the products was indicated from the two peaks at about 1.35 ppm in the ^{1}H nuclear magnetic resonance (NMR) spectra which represented the 27 protons on three *tert*-butyl groups. L1, L2, and L3 were obtained in good yields by routine deprotection of the *tert*-butyl groups in TFA/DCM. GdL1, GdL2, and GdL3 were obtained in moderate yields by heating $Gd_2(CO_3)_3$ with L1−L6 in water at 60 °Cat pH 6.0−6.5.

Relaxivities. The longitudinal relaxivities (r_1) at 400 MHz in degassed H2O/D_2O (9:1, v:v) at pH 7.0−7.4 at 25 °C were determined by plotting $1/T_{1,obs}$ against the concentration of GdL1−3 (Figure 1) and the relaxivities of GdL1, GdL2, and GdL3 were 4.74, 4.77, and 4.95 mM^{-1} s^{-1}, respectively (Table 1). The relaxivities were found to be in the normal range with one inner sphere water. Therefore, the complexes are expected to have eight coordinations attributed to the coordination of four nitrogens, three carboxylates, and one amide group from DO3A-amide to the Gd^{3+} center, leaving one coordination for one water molecule.

Table 1. Summary of Relaxivities of GdL1, GdL2, and GdL3

	r_1 (mM^{-1} s^{-1})[a]
	400 MHz
GdL1	4.74
GdL2	4.77
GdL3	4.95
GdDOTA	3.66

[a]Data was measured in degassed H_2O/D_2O (9:1) at pH 7.0−7.4.

All GdL1−3 showed higher relaxivities than the clinically used GdDOTA (DOTAREM, 3.66 mM^{-1} s^{-1} at 400 MHz). It is well-known that fast rotation is the limiting factor for small molecular Gd^{3+} complexes at high magnetic field strength.[34] The high relaxivities of GdL1−3 can be explained by their high molecular weight that slowed down their tumbling rate. This rate allowed a better matching with the Larmor frequency of water molecules and a higher relaxivity than those of low molecular weight complexes with fast tumbling rates.[34,35] The present of an ether linkage in GdL2 and GdL3 may enhance their relaxivity via enhancing the second or outer-sphere relaxivity by attracting water molecules to come closer to the Gd^{3+} center.[27] However, the relaxivities between GdL1−3 did not show a significant difference. The long PEO linkage of GdL3 only gave a 4% increment on relaxivity.

Binding Studies of Gd^{3+} Chelates to Serum Albumin. Serum albumin binding is one of the factors governing the pharmacokinetic properties of GdL1−3. Reversible binding of CA to HSA, the most abundant plasma protein, increases its retention time in blood and governs its biodistribution after administration. The binding property of GdL1−3 to bovine serum albumin (BSA), another most widely studied serum albumin due to its structural homology with HSA (76% sequence identity with HSA), was also studied for comparison. Both serum albumins bear tryptophan (Trp-214 for HSA and Trp-134, 212 for BSA) that can bind reversibly to a large number of endogenous and exogenous compounds.[36] Upon excitation at 280 nm, the tryptophan fluoresces are at 338 and 346 nm for HSA and BSA, respectively. The binding of MA with serum albumins has been studied through tryptophan emission-quenching experiment. The emission is quenched by the changes in protein conformation, subunit association, substrate binding, or protein denature.[37] It was found that addition of GdL1−3 or free MA to 4 μM HSA/BSA solution resulted in a significant decrease in tryptophan fluorescence (Figure 2). The tryptophan initial fluorescence intensities of HSA dropped to 44.7%, 43.5%, 34.3%, and 16.6%, whereas BSA dropped to 29.9%, 39.3%, 31.4%, and 8.3% for GdL1, GdL2, GdL3, and free MA, respectively, at a final concentration of 32 μM. The quenching constants can be derived from the fluorescence intensities by the Stern−Volmer equation:[38] $I_0/I = 1 + k_q\tau_0[Q] = 1 + K_{SV}[Q]$ where I_0 is the initial tryptophan fluorescence intensity of serum albumin, I is the tryptophan fluorescence intensity in the presence of quencher [Q], k is the quenching rate constant, K_{SV} is the dynamic quenching constant, τ_0 is the fluorescence lifetime of tryptophan in serum albumin taken at around 10^{-8} s, and [Q] is the concentration of the quencher. By plotting I_0/I versus [Q] (Figure S1), K_{SV} can be determined from the slope and hence the k_q can be determined. The number of binding sites per serum albumin (n) and the binding association constant (K) can be derived from the fluorescence intensity by the Scatchard equation:[39] $\Delta I/I_0[Q] = nK - K\Delta I/I_0$ where ΔI is the decreased

dx.doi.org/10.1021/bc5001356 | Bioconjugate Chem. 2014, 25, 1112−1123

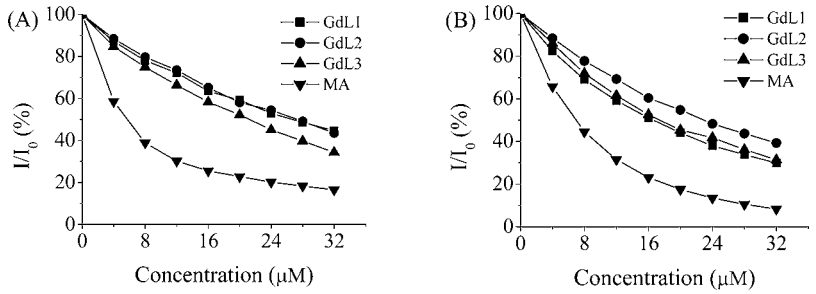

Figure 2. Relative fluorescence intensity of (A) 4 μM HSA at λ_{em} = 338 nm and (B) BSA at λ_{em} = 346 nm against increasing amount of quencher in 1 mM PBS solution at pH 7.4.

fluorescence intensity. By plotting $\Delta I/I_0/[Q]$ versus $\Delta I/I_0$ (Figure S2), K can be determined from the slope, while n can be determined from the ratio of the y-intercept to the slope. The calculated values of K_{SV}, k_q, K, and n of GdL1−3 toward HSA/BSA are given in Table 2. GdL1−3 showed a weaker fluorescence quenching toward HSA/BSA than that of free MA. The weak binding properties may be attributed to (i) the conversion of carboxylic acid into amide group that weakens the formation of hydrogen bondings at the binding site and (ii) the steric hindrance of bulky DOTA moieties. HSA is a 66 kDa monomeric protein composed of three structurally similar α-helical domains, I, II, and III. Two major binding sites can be distinguished for drugs binding according to the Suddlow classification scheme. Suddlow site I is located in the subdomain IIA that is considered to be a large and flexible region. Suddlow site II is located in the subdomain IIIA that is considered to be a hydrophobic pocket. Free MA was found to show high affinity toward the Suddlow site II.[40] It is possible that GdL1−3 are predominantly bound to the Suddlow site II while the larger and more flexible GdL2 and GdL3 give additional interaction to the Suddlow site I or they form hydrogen bondings with the peptide group present on the serum albumin. It was found that GdL1 showed a significantly stronger binding association constant K in BSA (4.05×10^4) than in HSA (2.81×10^4). This may be attributed to the interaction of the second tryptophan on BSA that is buried in a hydrophobic pocket located near the surface of the albumin.[41] The length of the hydrophobic ethane linker may fit the binding to this surface pocket and favor quenching. In addition, free MA may also bind to this pocket since the Stern−Volmer plot is upward-curving showing a static quenching behavior.[42]

Table 2. Summary of HSA/BSA Binding Constants and Parameters (K_{SV}, k_q, K, n) Derived for GdL1, GdL2, GdL3, and Free MA

		K_{SV} (M^{-1})	k_q (M^{-1} s^{-1})	K (M^{-1})	n
HSA	GdL1	3.84×10^4	3.84×10^{12}	2.81×10^4	1.15
	GdL2	3.70×10^4	3.70×10^{12}	1.94×10^4	1.42
	GdL3	5.36×10^4	5.36×10^{12}	2.25×10^4	1.53
	MA	1.55×10^5	1.55×10^{13}	1.90×10^5	0.98
BSA	GdL1	7.05×10^4	7.05×10^{12}	4.05×10^4	1.12
	GdL2	4.74×10^4	4.74×10^{12}	2.18×10^4	1.48
	GdL3	6.68×10^4	6.68×10^{12}	2.83×10^4	1.46
	MA	3.38×10^5	3.38×10^{13}	9.92×10^4	1.23

MTT Assay and Cellular Uptake Studies. Safety is the prime concern to evaluate the potential use of Gd^{3+} MRI CA. The high toxicity of Gd^{3+} complexes to living organism is mainly due to the free Gd^{3+} ions that interfere with the endogenous ions. The cytotoxicities of GdL1−3 on HeLa cells, one of the most commonly used human cell lines, were determined by standard MTT assay (Figure 3). GdDOTA, a commercially available MRI contrast agent, was also studied for comparison. After incubation at 37 °C for 24 h, it was found that GdL1−3 and GdDOTA showed low toxicities on HeLa cells and their viabilities were maintained over 80% at 0.5 mM of Gd^{3+}. GdL2 and GdL3 are slightly toxic at 1.0 mM so that their viabilities dropped to 76% and 69%, respectively. However, it is worth noting that the standard dosage of MRI CA for human is 1.25−100 μmol/kg (depending on the CA)[43] and the clearance of typical small molecule CA is completed within 24 h. GdL1−3 at 500 μM neither promotes cell growth nor causes significant cell death. Thus, the low acute cytotoxicities support in vivo trials of GdL1−3 in animal models.

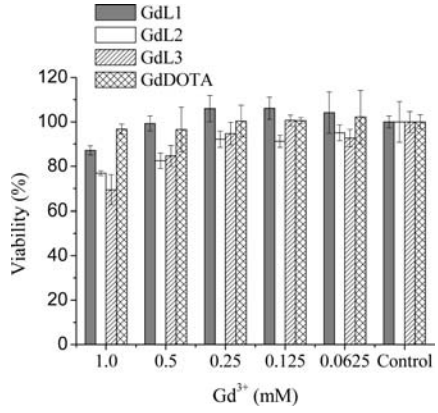

Figure 3. MTT assay of different concentrations of GdL1, GdL2, GdL3, and GdDOTA on HeLa cells after incubation at 37 °C for 24 h. Viability (%) shows the comparison between the growth inhibition effect in the presence and absence of Gd(III) complex. Error bars represent the standard deviation (±SD) on a triplicate analysis (n = 3).

The intensity of MRI signal is dependent on the amount of CA present in tissues. The cellular uptake ability of GdL1−3 was determined by incubating different concentrations of GdL1−3 with U87 cells. Linear concentration-dependent cellular uptakes of GdL1−3 and GdDOTA complexes on U87 cell line (Figure 4A) were observed. In addition, time-dependent cellular uptake of GdL1−3 showed a reduced uptake speed between 6 and 24 h of incubation (Figure 4B). To further investigate the role of different linkers of GdL1−3 in the amount of cellular uptake, the lipophilicity of GdL1−3 was determined by stirring the corresponding complex in a hexanol/PBS solution for 3 days. The UV−vis spectra before

dx.doi.org/10.1021/bc5001356 | Bioconjugate Chem. 2014, 25, 1112−1123

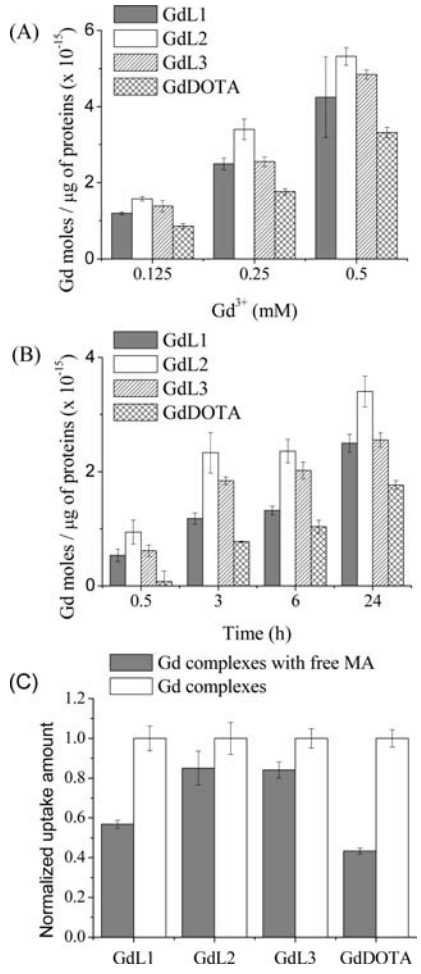

Figure 4. Cellular uptake amount of GdL1, GdL2, GdL3 and GdDOTA on U87 cells after incubation at 37 °C (A) for 24 h with different concentrations; (B) for different incubation time at 250 μM and (C) in the presence (solid bar) and absence (open bar) of 250 μM free MA. Error bars represent the standard deviation (±SD) on a triplicate analysis (n = 3).

and after stirring were compared (Figure S3) and the partition coefficients were calculated (Table S1). The lipophilicity (log P) is found to be on the order of GdL3 (0.102) ≈ GdL1 (0.087) > GdL2 (−0.006). This may suggest that the hydrophilic ether linker of GdL2 leads to a higher uptake than those of GdL1 and GdL3; however, the difference in lipophilicity is small (~5% difference), which is not conclusive for the explanation. The chain length and flexibility of the linker may also attribute to the difference in uptake. Further evaluation is needed on the role of the linkers.

GdL1−3 showed higher uptake amounts than that observed in GdDOTA. GdDOTA is known to have no specific binding to the receptor or protein in cell. However, these results on cellular uptake give limited information. Another cellular uptake experiment that incubates equal molar amounts of free MA with either GdL1−3 or GdDOTA was performed to further evaluate the uptake ability of GdL1−3. It is assumed that the molecular structure of MA governs the high uptake amount. In the presence of free MA, GdL1−3 may compete for the protein binding sites (e.g., COX-2) or the membrane binding sites (if any) of cells against the free MA. This would differentiate interactions of GdL1−3 to U87 cell by comparing the amounts of uptake in the presence and absence of free MA. GdDOTA was also included as a nonspecific reference for the comparison with GdL1−3. It was found that the amounts of cellular uptake for all complexes were significantly reduced in the presence of free MA (Figure 4C). Free MA is found to induce apotosis of liver cancer through the inhibition of caspase-3.[44] It is possible that part of the cells undergo apotosis and the ability of cellular uptake is reduced. The amounts of uptake were reduced in an ascending order of GdL2 (15.0%) ≈ GdL3 (15.9%) > GdL1 (43.2%) > GdDOTA (56.7%). Although the reason for the smaller uptake reduction of GdL1−3 than that of GdDOTA is not known and further mechanistic studies are needed, possible reasons are that the presence of mefenamic acid moiety on GdL1−3 may hinder free MA to induce apotosis or may be retained in the cell via interaction with proteins within the cell. The presence of ether/polyether group may have played a role in the high amount of cellular uptake of GdL2 and GdL3. Further investigation on the uptake mechanism, the uptaken location within the cell, or simulation of molecular docking of GdL1−3 to COXs is needed. Nevertheless, the high amount of uptake in these preliminary cellular uptake experiments supported the usage of GdL1−3 as in vivo MRI CAs.

In Vivo MR Imaging on U87 Xenograft. The U87 xenograft tumor transverse T_1-weighted MR images before and after intravenous injection of 0.1 mmol/kg GdDOTA and GdL1−3 to anesthetized nude mice are shown in Figure 5. Time-dependent MR signal intensity enhancements (IEs) of the tumor, kidney, and liver are shown in Figure 6. Transverse MR images of the kidney and liver images were also acquired to investigate the excretory pathway (Figures S4 and S5). GdL1−3 showed great IEs in the tumor, kidney, and liver throughout the 90 min scan. The margins of the U87 xenograft tumor were easily observed. The signal intensity of the periphery of the tumor increased more rapidly and strongly than the center. This might be attributed to the high interstitial fluid pressure in the tumor core.[45] Both the kidney and liver showed significant IEs suggesting that both organs are responsible for the excretion of GdL1−3. The renal pelvis, renal medulla, and renal cortex of the kidney could be identified depending on the intensity and position of the signals. The blood vessels of the liver could also be observed. These visible contrasts persisted at all ROIs for at least 90 min. On the contrary, after administration of GdDOTA, all tumor, kidney, and liver showed weaker intensities than those of GdL1−3. GdL1−3 showed different IE profiles and higher IEs than those of GdDOTA under the same dosage. In the tumor, GdDOTA showed a gradual enhancement in the first 60 min and a maximum IE of 1.18 ± 0.10, while GdL1, GdL2, and GdL3 showed high maximum IEs of 1.56 ± 0.13, 1.48 ± 0.11, and 1.44 ± 0.12, respectively, after initial administration and were constant at ca. 1.40 in the first 90 min. This IE trend was also observed in intravenous injection of MS-325 in a mouse with intracranial implantation of DBT cells.[46] The slow kinetics could be due to the binding of GdL1−3 with HSA that leads to a slow extravasation from tumor and a slow clearance from blood. In the kidney, GdDOTA showed a continuous decay of IE throughout the 90 min of the scan, while GdL1−3 only showed a fast decay in the first 15 min and then remained at a moderate level in the remaining time of the 90 min scan. The initial fast decay was possibly attributed by the high local concentration of GdL1−3 at the arterial phase whereas the later slow excretion rate might attribute to the binding of GdL1−3 with HSA proteins. In contrast to the kidneys, the liver IEs of GdL1−3 showed an initial decay in the first 15 min followed by

dx.doi.org/10.1021/bc5001356 | Bioconjugate Chem. 2014, 25, 1112−1123

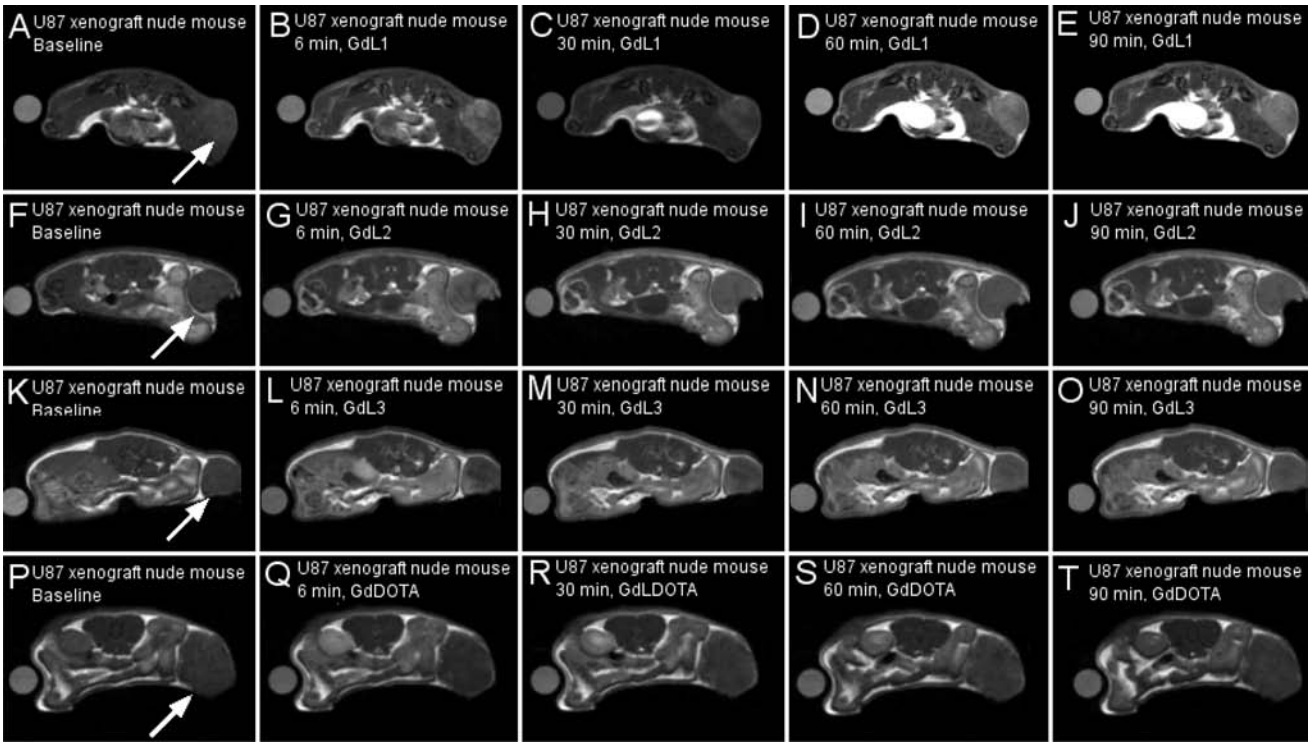

Figure 5. T1-weighted MR images of U87 xenograft nude mice taken at different time points. The acquired images were postprocessed using the maximum intensity projection (MIP) algorithm. White arrow indicates the U87 xenograft. (A–E) U87 xenograft nude mice images at baseline (A) and 6 min (B), 30 min (C), 60 min (D), and 90 min (E) postinjection of GdL1. (F–J) U87 xenograft nude mice images at baseline (F) and 6 min (G), 30 min (H), 60 min (I), and 90 min (J) postinjection of GdL2. (K–O) U87 xenograft nude mice images at baseline (K) and 6 min (L), 30 min (M), 60 min (N), and 90 min (O) postinjection of GdL3. (P–T) U87 xenograft nude mice images at baseline (P) and 6 min (Q), 30 min (R), 60 min (S), and 90 min (T) postinjection of GdDOTA.

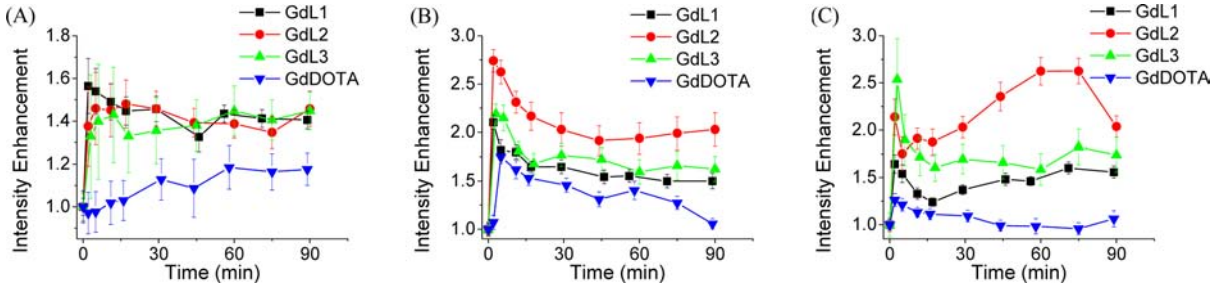

Figure 6. Time-dependent (a) tumor, (b) kidney cortex, and (c) liver IEs induced by 0.1 mmol/kg of GdL1 (■), GdL2 (●), GdL3 (▲), and GdDOTA (▼). Error bar represent the standard deviation (±SD) on the signal intensity analyzed by ImageJ.

a gradual build-up for 60 min. The high kidney and liver IEs of GdL2 reflected a more effective clearance than those of GdL1 and GdL3. This may suggest that the hydrophilic ether linker of GdL2 leads to a fast clearance while GdL3 bears a long and flexible hydrophilic ether linker may provide a better blood retention. The weak IEs at both the kidney and liver may be attributed to the large fraction of GdL3 in blood.

In Vivo MR Imaging on Arthritis Model. The high IEs in U87 xenograft mouse model suggested a low standard dosage for GdL1–3. Thus, 0.03 mmol/kg, the standard dosage of the blood pool agent Ablavar, formerly known as MS-325,[43] was used in AIA mouse model. RHL is the site of adjuvant injection where pathologic changes are much more severe than in the left hind limb. The signals in the RHL were significantly enhanced after intravenous injection of 0.03 mmol/kg of GdL1–3 (Figure 7A–O). The MR signals were easily observed and maintained within the first 2 h postadministration. At 24 h postadministration, no visible MR enhancements were observed for all GdL1–3 revealing that their clearance was almost complete (Figure S6). In contrast, 0.03 mmol/kg of GdDOTA only gave visible enhancement in the first 15 min postadministration (Figure 7P–T). Significant IE was observed when a standard dosage (0.1 mmol/kg) of GdDOTA was administrated, but the signals vanished rapidly within 120 min postadministration (Figure 7U–Y). The IE profiles of GdL1–3 were different from those of GdDOTA (Figure 8). GdL1–3 showed a gradual buildup of IE at the RHL and reached a maximum (1.35, 1.51, and 1.59 for GdL1, GdL2, and GdL3, respectively) at about 20 min postadministration, while GdDOTA showed a monoexponential decay after the maximum IE (1.29 and 1.93 for 0.03 and 0.1 mmol/kg of GdDOTA, respectively) was reached at about 3–7 min postadministration. Despite the higher IE that gave better contrast, the steady and long-lived IE provided a long optimal

dx.doi.org/10.1021/bc5001356 | Bioconjugate Chem. 2014, 25, 1112–1123

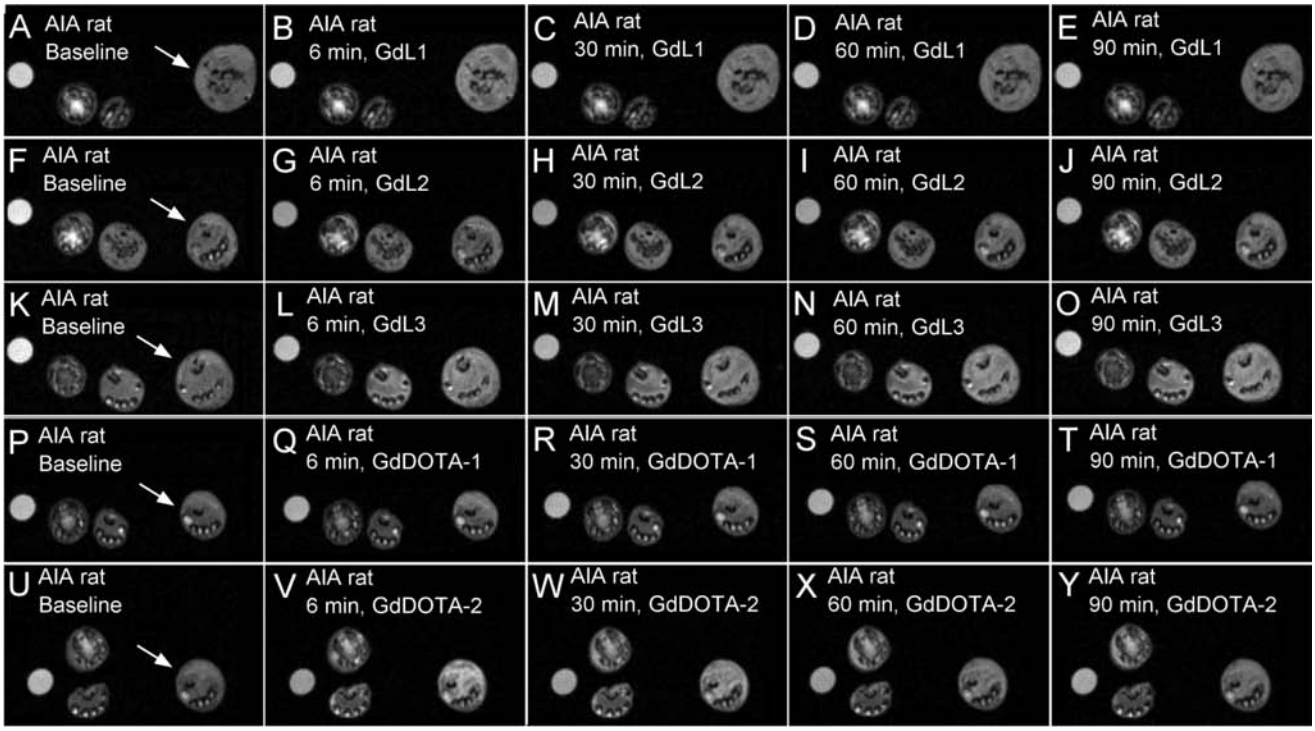

Figure 7. T1-weighted MR images of AIA rat taken at different time points. The acquired images were postprocessed using the maximum intensity projection (MIP) algorithm. White arrow indicates the RHL. 0.03 mmol/kg of GdDOTA is abbreviated as GdDOTA-1; 0.1 mmol/kg of GdDOTA is abbreviated as GdDOTA-2. (A–E) AIA rat images at baseline (A) and 6 min (B), 30 min (C), 60 min (D), and 90 min (E) postinjection of GdL1. (F–J) AIA rat images at baseline (F) and 6 min (G), 30 min (H), 60 min (I), and 90 min (J) postinjection of GdL2. (K–O) AIA rat images at baseline (K) and 6 min (L), 30 min (M), 60 min (N), and 90 min (O) postinjection of GdL3. (P–T) AIA rat images at baseline (P) and 6 min (Q), 30 min (R), 60 min (S), and 90 min (T) postinjection of 0.03 mmol/kg of GdDOTA. (U–Y) AIA rat images at baseline (U) and 6 min (V), 30 min (W), 60 min (X), and 90 min (Y) postinjection of 0.1 mmol/kg of GdDOTA.

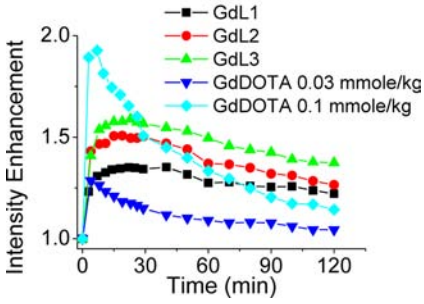

Figure 8. Time-dependent RHL IEs of AIA Wistar rats induced by 0.03 mmol/kg of GdL1 (■), GdL2 (●), GdL3 (▲), GdDOTA (▼), and 0.1 mmol/kg of GdDOTA (♦). Standard deviations (±SD, 0.12–0.24 for 0.03 mmol/kg of GdL1, GdL2, GdL3, GdDOTA, and 0.09–0.41 for 0.1 mmol/kg GdDOTA) on the signal intensity analyzed by ImageJ are omitted for simplicity.

detection time and stable MR signals throughout the MRI scan. A fast decay might give a large derivation of signal during the MRI scan. GdL3 showed the best MRI signal among GdL1–3. Its maximum IE was ca. 17% and 5% stronger than those observed in GdL1 and GdL2, respectively. Notably, the IE of 0.03 mmol/kg of GdL3 was ca. 31% stronger than that of 0.03 mmol/kg of GdDOTA at 120 min postadministration. Unlike the strong retention in U87 xenograft, IEs of GdL1–3 dropped slowly from 30 to 120 min after the initial boost. It is possible that retention of the complexes was weakened by the enhanced permeability of the vasculature at the arthritis joints that elevates the intraarticular pressure.[47] It has been reported that infiltration of abnormal serum proteins into the synovial owing to angiogenesis and microvascular lesions is common in RA.[48,49] The high serum protein content at the arthritis joint may explain the slow excretion rate of GdL1–3, while the high water content at the arthritis joint may reflect the higher local concentration of GdL3 than that of GdL1 via the formation of hydrogen bondings between the polyether linker and the surrounding water molecules.

■ CONCLUSIONS

In this study, three new GdDO3A-amide based MRI CAs conjugated to different linkers with MA were designed, prepared, and characterized. The relaxivities of GdL1–3 at high magnetic field strengths (400 MHz) were higher than that of GdDOTA, probably due to the higher MW of GdL1–3. They were found to bind HSA and BSA but weaker bindings to HSA/BSA than that of free MA, possibly due to the presence of bulky DO3A-amide moiety. In addition, they showed low cytotoxicities toward HeLa cells at 0.5 mM after incubation at 37 °C for 24 h. We also found that the uptake amount of Gd in U87 cells was positively related to the concentration of Gd complexes added in the incubation. In particular, GdL2 showed the highest amount of uptake, while GdL1–3 showed higher uptake amount than that of GdDOTA. In the presence of free MA, the cellular uptake amount of GdDOTA was reduced to a larger extent than those of GdL1–3. The presence of the mefenamic acid moiety on GdL1–3 may have an effect on the uptake mechanism. The MRI abilities of GdL1–3 were tested and they showed good retention in blood, high IEs on U87 xenograft, and pronounced inflammation in arthritis joint in in

dx.doi.org/10.1021/bc5001356 | Bioconjugate Chem. 2014, 25, 1112–1123

vivo MRI studies at 4.7 T magnetic field strength. Their MRI signals at tumor, kidney, and liver were observable for more than 90 min postadministration in the U87 xenograft model, while their signals at arthritis joint (RHL) were significantly stronger than those of GdDOTA at 120 min postadministration in the AIA model. In MRI studies of both the U87 and AIA models, all the complexes with the MA moieties showed a longer imaging time window than that of GdDOTA, and better contrast enhancement was observed in the tumor and the arthritis joint. To conclude, this study has demonstrated the potential use of NSAIDs as MRI targeting moieties and the effects of the three linkers on the MRI contrast agent property. The different linkers have minor effects on HSA/BSA binding, cytotoxicity, cellular uptake amount, lipophilicity, and biodistribution. It is worth screening the linker to maximize the efficiency of MRI CA. The combination of MRI and the antiinflammatory ability of NSAID could be a prospective model of theranostics for MRI to assess inflammation-related diseases.

EXPERIMENTAL SECTION

General Methods. All chemicals and solvents were of analytical grade and used without further purification unless otherwise stated. All buffer components were of biological grade and used as received. The compounds *tert*-butylbromoacetate, chloroacetyl chloride, *N*,*N*′-dicyclohexylcarbodiimide (DCC), ethylenediamine, *N*-hydroxysuccinimide (NHS), mefenamic acid (MA), trifluoroacetic acid (TFA), and 4,7,10-trioxa-1,13-tridecanediamine were purchased from Sigma-Aldrich; 1,4,7,10-tetraazacyclododecane and gadolinium carbonate were purchased from Strem; 2,2′-oxidiethylamine was purchased from TCI; human serum albumin (HSA) and bovine serum albumin (BSA) were purchased from Sigma-Aldrich and used as received. The ^{1}H and ^{13}C NMR spectra were recorded on a Bruker DPX300 Bruker FT-NMR spectrometer and an AV400 Bruker FT-NMR spectrometer. Chemical shifts (δ, ppm) were reported relative to tetramethylsilane (TMS). Both positive and negative modes of electron spray ionization (ESI) mass spectra were recorded on a Finnigan MAT LCQ mass spectrometer. ESI samples were prepared in HPLC grade solvents and filtered through a 0.20 μm filter before acquisition. Tri-*tert*-butyl-1,4,7,10-tetraazacyclododecane-1,4,7-triacetate (tricyc) was prepared according to reported procedures.[33] The absence of free Gd^{3+} for all complexes was confirmed by xylenol orange test according to reported procedures to rule out overestimation of relaxivity, cytotoxicity, and the amount of cellular uptake.[50]

Synthesis of GdL1−3. *N-[2-(2-Chloro-acetylamino)-ethyl]-2-(2,3-dimethyl-phenylamino)-benzamide (2).* The synthetic procedures of (2) were modified according to the literature.[51−53] Mefenamic acid (3.00 g, 12.4 mmol) and NHS (3.43 g, 29.8 mmol) were heated to dissolve in 75 mL DMF. DCC (3.08 g, 14.88 mmol) was added and the mixture was stirred at room temperature under nitrogen for 5 h. The resultant yellow mixture was filtered and dried under vacuum to give a yellowish oil. The oil was purified by flash column chromatography on silica using $CHCl_3$ as the eluate to yield (1). (1) was dissolved in 50 mL DCM and added dropwise to an ethylenediamine (8.27 mL, 124 mmol) solution over 30 min. The mixture was stirred at room temperature under nitrogen for 24 h. The resultant mixture was filtered and washed with brine (100 mL × 3). The organic layer was dried over anhydrous $Mg(SO)_4$ and filtered into a 25 mL NaOH solution (1.49 g, 37.2 mmol). The bilayer solution was stirred at 0 °C for 15 min and chloroacetyl chloride (2.98 mL, 37.2 mmol) was then added dropwise into the solution. The mixture was stirred at 0 °C for another 15 min and then at room temperature for 12 h. The resultant organic layer was collected.

The crude product was purified by column chromatography on silica using $CHCl_3$ as the eluate to yield (2). Yield: 2.77 g (62%). ^{1}H NMR (400 MHz, $CDCl_3$): δ 9.28 (s, 1H), 7.63 (t, 1H, J = 5.28 Hz), 7.49 (dd, 1H, J = 7.93 and 1.39 Hz), 7.41 (t, 1H, J = 5.26 Hz), 7.20 (td, 1H, J = 7.80 and 1.45 Hz), 7.17 (d, 1H, J = 7.77 Hz), 7.08 (t, 1H, J = 7.58 Hz), 6.97 (d, 1H, J = 7.38 Hz), 6.93 (dd, 1H, J = 8.44 and 0.81 Hz), 6.66 (t, 1H, J = 7.49 and 0.96 Hz), 3.99 (s, 2H), 3.63−3.59 (m, 2H), 3.55−3.51 (m, 2H), 2.33 (s, 3H), 2.21 (s, 3H). ^{13}C NMR (400 MHz, $CDCl_3$): δ 170.8, 167.6, 147.2, 139.3, 138.0, 132.5, 130.8, 127.8, 125.8, 125.7, 120.9, 116.8, 116.1, 114.8, 42.5, 40.5, 39.7, 20.6, 13.8. ESI-MS m/z for ($M+Na^+$) calcd 382.1, found 360.1. For ($3M+K^++H^+$) calcd 558.7, found 559.4. For ($2M+Na^+$) calcd 741.2, found 740.7.

N-{2-[2-(2-Chloro-acetylamino)-ethoxy]-ethyl}-2-(2,3-dimethyl-phenylamino)-benzamide (3). The synthetic procedures were similar to those of (2) except that 2,2′-oxidiethylamine (2.64 g, 24.8 mmol) was used instead of ethylenediamine. Yield: 3.16 g (63%). ^{1}H NMR (300 MHz, $CDCl_3$): δ 7.46 (d, 1H, J = 7.85 Hz), 7.22−7.14 (m, 2H), 7.12−7.00 (m, 2H), 7.00−6.85 (m, 3H), 6.67 (t, 1H, J = 7.42 Hz), 3.98 (s, 2H), 3.63 (br, 4H), 3.60−3.53 (m, 2H), 3.53−3.45 (m, 2H), 2.31 (s, 3H), 2.20 (s, 3H). ^{13}C NMR (300 MHz, $CDCl_3$): δ 169.8, 166.2, 147.0, 139.4, 137.9, 132.2, 130.6, 127.6, 125.7, 125.5, 120.7, 116.65, 116.62, 114.7, 69.4, 69.1, 42.5, 39.4, 20.6, 13.8. ESI-MS m/z for ($M+Na^+$) calcd 426.2, found 426.2. For ($2M+Na^+$) calcd 829.3, found 828.7.

N-[3-(2-{2-[3-(2-Chloro-acetylamino)-propoxy]-ethoxy}-ethoxy)-propyl]-2-(2,3-dimethyl-phenylamino)-benzamide (4). The synthetic procedures were similar to those of (2) except that 4,7,10-trioxa-1,13-tridecanediamine (5.46 g, 24.8 mmol) was used instead of ethylenediamine. Yield: 1.10 g (17% based on mefenamic acid). ^{1}H NMR (300 MHz, $CDCl_3$): δ 9.36 (s, 1H), 7.43 (d, 1H, J = 7.62 Hz), 7.27 (br, 2H), 7.15−7.08 (m, 2H), 7.00 (t, 1H, J = 7.60 Hz), 6.90−6.85 (m, 2H), 6.61 (t, 1H, J = 7.51 Hz), 3.94 (s, 2H), 3.61−3.52 (m, 8H), 3.52−4.48 (m, 6H), 3.34 (q, 2H, J = 5.74 Hz), 2.26 (s, 3H), 2.16 (s, 3H), 1.85 (p, 2H, J = 5.87 Hz), 1.72 (p, 2H, J = 5.89 Hz). ^{13}C NMR (300 MHz, $CDCl_3$): δ 169.4, 165.7, 146.8, 139.5, 137.7, 131.7, 130.4, 127.5, 125.5, 125.2, 120.4, 117.0, 116.4, 114.4, 70.35, 70.25, 70.11, 70.08, 42.5, 38.46, 38.35, 28.7, 28.4, 20.5, 13.7. ESI-MS m/z for ($M-H^-$) calcd 518.2, found 518.8. For ($M+2Na^+-3H^-$) calcd 562.2, found 564.4.

[4,7-Bis-tert-butoxycarbonylmethyl-10-({2-[2-(2,3-dimethyl-phenylamino)-benzoylamino]-ethylcarbamoyl}-methyl)-1,4,7,10tetraaza-cyclododec-1-yl]-acetic acid tert-butyl ester (5). A mixture of tricyc (1.0 g, 1.94 mmol), K_2CO_3 (804 mg, 5.83 mmol) and (2) (838 mg, 2.33 mmol) was stirred in 50 mL dry acetonitrile at 60 °C under nitrogen for 2 days. The resultant mixture was filtered and dried under reduced pressure. The residue was purified by chromatography on silica (eluent gradient from $CHCl_3$ to $CHCl_3$/MeOH, 9.5:0.5) to yield (5). Yield: 537 mg (33%). ^{1}H NMR (300 MHz, $CDCl_3$): δ 9.67 (s, 1H), 8.68 (br, 1H), 8.41 (br, 1H), 8.11 (d, 1H, J = 7.42 Hz), 7.16−7.09 (m, 2H), 7.00 (t, 1H, J = 7.59 Hz), 6.86 (t, 2H, J = 8.71 Hz), 6.73 (t, 1H, J = 7.11 Hz), 3.70−1.60 (m, 34H), 1.42 (s, 9H), 1.37 (s, 18H). ^{13}C NMR (400 MHz, $CDCl_3$): δ 172.4, 172.1, 171.9, 170.2, 146.9, 140.3, 137.8, 131.8, 130.2, 129.8, 125.6, 124.8, 120.1, 117.3, 116.6, 114.2, 82.0, 56.1, 55.7, 53.0−

dx.doi.org/10.1021/bc5001356 | *Bioconjugate Chem.* 2014, 25, 1112−1123

47.0, 39.7, 38.7, 28.2, 20.7, 14.0. ESI-MS m/z for ($M-{}^{t}Bu+Na^{+}$) calcd 804.5, found 804.4. For ($M+H^{+}$) calcd 838.6, found 838.5. For ($M+Na^{+}$) calcd 860.5, found 860.4.

{4,7-Bis-tert-butoxycarbonylmethyl-10-[(2-{2-[2-(2,3-dimethyl-phenylamino)-benzoylamino]-ethoxy}-ethylcarbamoyl)-methyl]-1,4,7,10tetraaza-cyclododec-1-yl}-acetic acid tert-butyl ester (6). The synthetic procedures were similar to those of (5) except that (3) (941 mg, 2.33 mmol) was used instead of (2). Yield: 987 mg (48%). ^{1}H NMR (400 MHz, $CDCl_3$): δ 9.55 (s, 1H), 8.25 (t, 1H, J = 5.21 Hz), 8.00 (t, 1H, J = 5.28 Hz), 7.96 (d, 1H, J = 7.83 Hz), 7.10−7.06 (m, 2H), 6.96 (t, 1H, J = 7.63 Hz), 6.86−6.81 (m, 2H), 6.67 (t, 1H, J = 7.35 Hz), 3.70−3.50 (m, 6H), 3.50−1.50 (m, 32H), 1.37 (s, 9H), 1.35 (s, 18H). ^{13}C NMR (400 MHz, $CDCl_3$): δ 172.3, 171.9, 170.0, 146.8, 140.0, 137.8, 131.7, 130.2, 129.3, 125.5, 124.9, 120.0, 117.0, 116.7, 114.3, 81.8, 81.7, 69.4, 68.6, 56.2, 55.6, 55.5, 53.9−47.0, 39.4, 39.1, 27.9, 27.8, 20.6, 13.9. ESI-MS m/z for ($M-{}^{t}Bu+Na^{+}$) calcd 848.6, found 848.4. For ($M+Na^{+}$) calcd 904.6, found 904.4.

[4,7-Bis-tert-butoxycarbonylmethyl-10-({3-[2-(2-{3-[2-(2,3-dimethyl-phenylamino)-benzoylamino]-propoxy}-ethoxy)-ethoxy]-propylcarbamoyl}-methyl)-1,4,7,10tetraaza-cyclododec-1-yl]-acetic acid tert-butyl ester (7). The synthetic procedures were similar to those of (5) except that (4) (1.21 g, 2.33 mmol) was used instead of (2). Yield: 1.22 g (63%). ^{1}H NMR (400 MHz, $CDCl_3$): δ 9.38 (s, 1H), 7.97 (t, 1H, J = 5.34 Hz), 7.52 (d, 1H, J = 7.88 Hz), 7.47 (t, 1H, J = 4.77 Hz), 7.08−7.04 (m, 2H), 6.93 (t, 1H, J = 7.58 Hz), 6.82−6.78 (m, 2H), 6.59 (t, 1H, J = 7.42 Hz), 3.56−3.38 (m, 14H), 3.38−1.50 (m, 36H), 1.34 (s, 9H), 1.33 (s, 18H). ^{13}C NMR (400 MHz, $CDCl_3$): δ 172.3, 171.9, 171.3, 169.4, 146.7, 139.6, 137.7, 131.6, 130.2, 128.0, 125.4, 125.0, 120.2, 116.9, 116.7, 114.3, 81.6, 81.5, 70.3, 70.2, 70.1, 69.8, 69.1, 56.0, 55.5, 55.4, 53.0−47.0, 38.1, 36.5, 29.4, 29.1, 28.8, 27.8, 27.7, 20.5, 13.7. ESI-MS m/z for ($M+H^{+}$) calcd 998.7, found 998.5. For ($M+Na^{+}$) calcd 1020.6, found 1020.5.

[4,7-Bis-carboxymethyl-10-({2-[2-(2,3-dimethyl-phenylamino)-benzoylamino]-ethylcarbamoyl}-methyl)-1,4,7,10tetraaza-cyclododec-1-yl]-acetic acid (L1). (5) (500 mg, 0.60 mmol) was stirred in a 20 mL mixture of DCM and trifluoroacetic acid (TFA) (1:1, v:v) at room temperature for 24 h. The resultant mixture was dried under vacuum. The residue was washed with DCM and diethyl ether to yield (L1). Yield: 364 mg (91%). ^{1}H NMR (400 MHz, MeOD): δ 7.51 (s, 1H), 7.05 (s, 1H), 6.95−6.89 (m, 2H), 6.80 (d, 1H, J = 6.54 Hz), 6.66−6.57 (m, 2H), 3.70−2.80 (m, 28H), 2.16 (s, 3H), 2.01 (s, 3H). ^{13}C NMR (400 MHz, MeOD): δ 172.2, 148.2, 140.8, 139.2, 133.3, 131.7, 129.7, 127.0, 126.8, 122.1, 118.4, 118.2, 115.5, 56.4, 51.6, 50.7, 40.5, 40.0, 20.7, 14.2. ESI-MS m/z for ($M+H^{+}$) calcd 670.4, found 670.1. For ($M+Na^{+}$) calcd 692.3, found 692.3. For ($M+K^{+}$) calcd 708.3, found 708.1. For ($M+Na^{+}+K^{+}-H^{+}$) calcd 730.3, found 730.1. For ($M+2Na^{+}+K^{+}-2H^{+}$) calcd 752.3, found 752.1.

{4,7-Bis-carboxymethyl-10-[(2-{2-[2-(2,3-dimethyl-phenylamino)-benzoylamino]-ethoxy}-ethylcarbamoyl)-methyl]-1,4,7,10tetraaza-cyclododec-1-yl}-acetic acid (L2). The synthetic procedures were similar to those of (L1) except that (6) (529 mg, 0.60 mmol) was used instead of (5). Yield: 411 mg (96%). ^{1}H NMR (400 MHz, D_2O): δ 7.46 (s, 1H), 7.00−6.65 (m, 3H), 6.65−6.40 (m, 3H), 4.50−2.50 (m, 32H), 1.93 (s, 3H), 1.85 (s, 3H). ^{13}C NMR (400 MHz, MeOD): δ 172.0, 147.9, 140.7, 139.2, 133.2, 131.6, 129.6, 127.0, 126.8, 121.9, 119.6, 118.3, 115.6, 70.4, 69.9, 56.0, 51.3, 40.4, 20.7, 14.0. ESI-MS m/z for ($M+K^{+}-2H^{+}$) calcd 750.3, found 750.9. For ($M+Na^{+}+K^{+}-3H^{+}$) calcd 772.3, found 774.7.

[4,7-Bis-carboxymethyl-10-({3-[2-(2-{3-[2-(2,3-dimethyl-phenylamino)-benzoylamino]-propoxy}-ethoxy)-ethoxy]-propylcarbamoyl}-methyl)-1,4,7,10tetraaza-cyclododec-1-yl]-acetic acid (L3). The synthetic procedures were similar to those of (L1) except that (7) (598 mg, 0.60 mmol) was used instead of (5). Yield: 398 mg (80%). ^{1}H NMR (400 MHz, MeOD): δ 7.58 (d, 1H, J = 7.64 Hz), 7.19 (t, 1H, J = 8.06 Hz), 7.10−7.00 (m, 2H), 6.91 (d, 1H, J = 7.07 Hz), 6.82 (d, 1H, J = 8.32 Hz), 6.73 (t, 1H, J = 7.51 Hz), 3.80−2.90 (m, 40H), 2.28 (s, 3H), 2.15 (s, 3H), 1.87 (p, 2H, J = 6.18 Hz), 1.76 (br, 2H). ^{13}C NMR (400 MHz, $CDCl_3$): δ 171.7, 147.8, 140.8, 139.1, 133.1, 131.3, 129.4, 127.0, 126.6, 121.6, 118.9, 118.3, 115.6, 71.3, 71.1, 71.0, 70.1, 69.9, 56.2, 51.1, 38.4, 38.3, 30.4, 30.1, 20.8, 14.1. ESI-MS m/z for ($M-H^{+}$) calcd 828.5, found 828.7. For ($M+K^{+}-2H^{+}$) calcd 866.4, found 866.5.

(GdL1). L1 (200 mg, 0.30 mmol) was dissolved in 20 mL H_2O. The pH was adjusted to 6.0−6.5 by adding 0.1 M NaOH. Gadolinium carbonate (0.18 mmol) was added and stirred at 60 °C for 12 h. The resultant mixture was filtered and purified by chromatography on silica (eluent gradient from MeOH to MeOH/H_2O, 8:2). The crude product was dried, dissolved in minimum amount of MeOH and filtered through a 0.20 μm cellulose acetate filter (Advantec) repeatedly until a clear solution was obtained. The crude product was then recrystallized from MeOH/diethyl ether to yield (GdL1). Yield: GdL1 173 mg (70%). ESI-MS m/z for ($M+H^{+}$) calcd 825.3, found 825.3. For ($M+Na^{+}$) calcd 847.2, found 847.1.

(GdL2). The synthetic procedures were similar to those of (GdL1) except that (L2) (214 mg, 0.3 mmol) was used instead of (L1). Yield: GdL2 172 mg (66%). ESI-MS m/z for ($M+Na^{+}$) calcd 891.3, found 891.3. For ($2M+Na^{+}$) calcd 1759.6, found 1759.3.

(GdL3). The synthetic procedures were similar to those of (GdL1) except that (L3) (217 mg, 0.3 mmol) was used instead of (L1). Yield: GdL3 166 mg (56%). ESI-MS m/z for ($M+H^{+}$) calcd 985.4, found 985.4. For ($M+Na^{+}$) calcd 1007.4, found 1007.3. For ($2M+H^{+}$) calcd 1969.7, found 1969.4.

Measurements of Relaxivity. GdL1−3 at concentrations of 5, 3, and 1 mM were prepared in degassed H_2O/D_2O (9:1, v:v) at pH 7.0−7.4. Relaxometric measurements were performed on a Bruker AV 400 NMR spectrometer using standard inversion recovery pulse sequence with T_1 delay time points ranging from 5 ms to 5 s with a TR > 5 T_1 at 25 °C. The longitudinal relaxivity, r_1, was determined from the slope by plotting the observed relaxation rate ($1/T_{1,obs}$) against the concentration of GdL1−3 with a linear regression (R^2) greater than 0.99. The slope of the linear fit was recorded as r_1.

Serum Albumin Binding Studies. The binding of GdL1−3 and MA with serum albumin was studied from a tryptophan emission-quenching experiment that has been described in detail elsewhere.[54] The quenching of tryptophan fluorescence intensity at 338 and 346 nm for 4 μM HSA/BSA in 1 mM PBS solution upon excitation at 280 nm. The quenching of the emission intensity was monitored upon successive addition of GdL1−3 or free MA as quenchers with increasing concentration by a Horiba Jobin Yvon Fluorolog-3-TCSPC spectrofluorimeter with 2 nm emission and excitation slit widths.

MTT Assay. HeLa cell line was grown in a 96-well polystyrene flat bottom tissue culture-treated plate with minimum essential medium eagle (MEM, Invitrogen) with 10% fetal bovine serum (FBS, Invitrogen) in a 5% CO_2

incubator at 37 °C. The number of cells in each well was approximately 8.0×10^3 cells. The culture media were removed and 100 μL MEM of GdL1−3 with concentrations of 1000, 500, 250, 125, 62.5, 31.25, or 0 μM was added and incubated for 19 h (n = 3). 20 μL MTT solution (5.0 mg mL^{-1}) was added to each cell-containing well in the dark to avoid photobleaching. The plate was then incubated for 5 h. The culture media were carefully removed by syringe. 200 μL of DMSO was added to each well and pipetted up and down to dissolve crystals. After incubation at 37 °C for 5 min, the absorbance at 570 nm was measured with a DG-3022a ELISA-Reader and expressed as a percentage relative to control cells.

Measurements of Cellular Uptake. U87 cell lines were purchased from American Type Culture Collection (ATCC, Manassas, VA) and grown in a 24-well polystyrene flat bottom tissue-culture treated plate with MEM (with 10% w/w FBS) in a 5% CO_2 incubator at 37 °C. The number of cells in each well was approximately 6.0×10^4 cells. The culture media were removed and 500 μL MEM of GdL1−3 with concentrations of 500, 250, or 125 μM was added and incubated for 24 h (n = 3). The culture media were removed and the cells were rinsed carefully with 250 μL phosphate buffered saline (PBS) three times. 250 μL radio-immunoprecipitation assay (RIPA) buffer (Sigma-Aldrich) was added to each well and incubated on ice for 15 min to lyse the cells. 25 μL of each sample solution was added to 200 μL working reagent of BCA protein assay (The Thermo Scientific) in a 96-well plate and incubated at 37 °C for 30 min. The absorbance at 570 nm was measured with a DG-3022a ELISA-Reader and expressed as the total protein concentration in each well (protein μg mL^{-1}). 200 μL of each residue sample solution was collected and incubated with concentrated nitric acid 69.5% (for trace analysis, Fluka) at 80 °C for 5 h. Samples were then diluted to 10 mL by 1% nitric acid with 40 ppb of indium as an internal standard and analyzed by Agilent 7500a ICP-MS with ICP-MS Top installed. The procedures of measuring time-dependent cellular uptake were similar to those of concentration-dependent cellular uptake except that 500 μL MEM containing 250 μM of GdL1−3 and GdDOTA was used and the cells were harvested after incubation for 30 min, 1 h, 3 h, 6 h, and 24 h, respectively. The procedures of measuring competitive cellular uptake by free MA were similar to those of measuring concentration dependent cellular uptake, except that 500 μL MEM containing 250 μM of GdL1−3 and GdDOTA was coincubated with 250 μM of free MA.

Preparation of Animal Model. For U87 xenograft, male Balb/c nude mice (18−22 g) aged 6−8 weeks old were obtained from PearL Materia Medica Development (Shenzhen) Ltd. The mice were housed in pathogen-free conditions meeting the National Standard for the Quality of Laboratory Animal of PRC. They were allowed free access to distilled water and fed on a commercial diet with alternating 12 h of light/12 h of darkness at 23 °C and humidity of 55%. The mice were treated in accordance with the guidelines of the Animal Ethic Committee of The Hong Kong Polytechnic University. A PBS suspension of U87 cells containing approximately 1×10^7 cell per mL was prepared. The nude mice were anesthetized by isofluorane/oxygen gas. Approximately 300 μL of the suspension was injected subcutaneously into the right gluteal region of the nude mice. The tumors were allowed to grow for 20−25 days under supervision before MRI experiments. For AIA, Male Wistar rats (175−225 g) were obtained and cared for under the same conditions except that they were housed in a normal room. Approximately 0.05 mL Freund's complete adjuvant containing 10 mg mL^{-1} of *Mycobacterium butyricum* (Sigma) was injected subcutaneously into the paw of the right hind limb (RHL). The progression of the joint inflammation was monitored by measuring the diameter of the ankle joint with a digital caliper and the weights of the rats were also measured at least 3 times a week. The maximum inflammation was achieved after 13−15 days postinjection and the rats were subjected to MRI experiments.

In Vivo MR Imaging. MR scans were performed on a Bruker Biospec 4.7 T/30 cm scanner with a 50-mm-diameter quadrature volume coil for transmission/reception. The xenografted nude mice were anesthetized by 1.5−2.5% isofluorane in pure oxygen gas and fixed to an acrylic animal bed by adhesive tape to reduce body movement. A tube containing 0.1 mM GdDOTA was placed next to the mice as a phantom reference. The respiratory rate was monitored and kept at 60−120 times per minute by adjusting the isofluorane dosage. GdL1−3 (0.1 mmol/kg) was prepared in saline and administrated through tail vein injection (n = 1 per compound). T_1-weighted images were acquired by a multislice and multiecho (MSME) sequence with the following parameters: TR = 300.0 ms, TE = 11.0 ms, excitation flip angle (FA) = 90°, slice thickness (SI) = 1.0 mm, field of view (FOV) = 4.0 cm × 4.0 cm centered at the tumor, number of averages (NA) = 4, and matrix size = 128 × 128. The acquisition parameters were the same for AIA rat except that TR = 400 ms, SI = 2 mm, FOV centered at the two paws of the hind limb, and 0.03 mmol/kg of GdL1−3 was administrated through tail vein injection (n = 1 per compound). MR scans of 0.03 and 0.1 mmol/kg of GdDOTA were also done as references (n = 1 per concentration). Postprocessing was done on the T_1-weighted precontrasted MR images of the tumor, kidney, and liver using the maximum intensity projection (MIP) algorithm. The precontrasted MR images are denoted as 0 min. The T_1-weighted postcontrasted MR images were continuously taken for at least 90 min and an extra time point at 24 h was taken to monitor the total clearance of the complexes. Images were analyzed by ImageJ.[55] Fluctuations on signal intensity (SI) were corrected by $ROI' = SI_{ROI}/SI_{GdDOTA}$, where ROI′ is the corrected signal intensity of the region of interest (ROI). SI_{ROI} is the raw averaged signal intensity of ROI. SI_{GdDOTA} is the averaged signal intensity of the 0.1 mM GdDOTA reference phantom. The ROI at time t is expressed by $IE = (ROI_t' - ROI_0')/ROI_0'$, where ROI_t' is the corrected signal intensity of the ROI at time t. ROI_0' is the corrected signal intensity of the ROI at time 0. The SI at the tumor, kidney, and liver was analyzed in U87 xenograft model, while the RHL was analyzed in AIA model.

■ ASSOCIATED CONTENT

Supporting Information

HSA/BSA Stern−Volmer plot and Scatchard plot of GdL1−3 and free MA; T_1-weighted kidney and liver MR images on U87 xenograft nude mice before and after administration of GdL1−3; Lipophilicity data; T_1-weighted RHL MR images on AIA Wistar rats after 24 h administration of GdL1−3. This material is available free of charge via the Internet at http://pubs.acs.org.

■ AUTHOR INFORMATION

Corresponding Author

*E-mail wing-tak.wong@polyu.edu.hk.

Notes

The authors declare no competing financial interest.

■ ACKNOWLEDGMENTS

This work was financially supported by the Hong Kong Research Grants Council and The University of Hong Kong. We acknowledge the provision of Horiba Jobin Yvon Fluorolog-3-TCSPC spectrofluorimeter facilities by City University of Hong Kong. Arthur H−H. Leung acknowledges the receipt of a postgraduate studentship from The University of Hong Kong and thanks Dr. Cornelia W−Y. Man for technical assistance in biological work.

■ REFERENCES

(1) Thun, M. J., Henley, S. J., and Patrono, C. (2002) Nonsteroidal anti-inflammatory drugs as anticancer agents: mechanistic, pharmacologic, and clinical issues. *J. Natl. Cancer Inst. 94*, 252−66.

(2) Baron, J. A., and Sandler, R. S. (2000) Nonsteroidal anti-inflammatory drugs and cancer prevention. *Annu. Rev. Med. 51*, 511−23.

(3) Rodríguez, L. A. G., and Huerta-Alvarez, C. (2001) Reduced risk of colorectal cancer among long-term users of aspirin and nonaspirin nonsteroidal antiinflammatory drugs. *Epidemiology 12*, 88−93.

(4) Borrero, C. G., Mountz, J. M., and Mountz, J. D. (2011) Emerging MRI methods in rheumatoid arthritis. *Nat. Rev. Rheumatol. 7*, 85−95.

(5) Vane, J. R. (1971) Inhibition of prostaglandin synthesis as a mechanism of action for aspirin-like drugs. *Nat. New Biol. 231*, 232−5.

(6) Ferreira, S. H., Moncada, S., and Vane, J. R. (1971) Indomethacin and aspirin abolish prostaglandin release from the spleen. *Nat. New Biol. 231*, 237−9.

(7) Smith, J. B., and Willis, A. L. (1971) Aspirin selectively inhibits prostaglandin production in human platelets. *Nat. New Biol. 231*, 235−7.

(8) Kopp, E., and Ghosh, S. (1994) Inhibition of NF-κB by sodium salicylate and aspirin. *Science 265*, 956−9.

(9) Pillinger, M. H., Capodici, C., Rosenthal, P., Kheterpal, N., Hanft, S., Philips, M. R., and Weissmann, G. (1998) Modes of action of aspirin-like drugs: Salicylates inhibit Erk activation and integrin-dependent neutrophil adhesion. *Proc. Natl. Acad. Sci. U.S.A. 95*, 14540−5.

(10) Yin, M.-J., Yamamoto, Y., and Gaynor, R. B. (1998) The anti-inflammatory agents aspirin and salicylate inhibit the activity of IκB kinase-β. *Nature 396*, 77−80.

(11) Xie, W. L., Chipman, J. G., Robertson, D. L., Erikson, R. L., and Simmons, D. L. (1991) Expression of a mitogen-responsive gene encoding prostaglandin synthase is regulated by mRNA splicing. *Proc. Natl. Acad. Sci. U.S.A. 88*, 2692−6.

(12) Kujubu, D. A., Fletcher, B. S., Varnum, B. C., Lim, R. W., and Herschman, H. R. (1991) TIS10, a Phorbol ester tumor promoter-inducible mRNA from Swiss 3T3 cells, encodes a novel prostaglandin synthase/cyclooxygenase homologue. *J. Biol. Chem. 266*, 12866−72.

(13) Aggarwal, B. B., Shishodia, S., Sandur, S. K., Pandey, M. K., and Sethi, G. (2006) Inflammation and cancer: How hot is the link? *Biochem. Pharmacol. 72*, 1605−21.

(14) Laurent, S., Elst, L. V., Fu, Y., and Muller, R. N. (2004) Synthesis and physicochemical characterization of Gd-DTPA-B(sLe^x)-A, a new MRI contrast agent targeted to inflammation. *Bioconjugate Chem. 15*, 99−103.

(15) Uddin, M. J., Crews, B. C., Ghebreselasie, K., Huda, I., Kingsley, P. J., Ansari, M. S., Tantawy, M. N., Reese, J., and Marnett, L. J. (2011) Fluorinated COX-2 inhibitors as agents in PET imaging of inflammation and cancer. *Cancer. Prev. Res. 4*, 1536−45.

(16) Schmidt, G. P., Reiser, M. F., and Baur-Melnyk, A. (2009) Whole-body MRI for the staging and follow-up of patients with metastasis. *Eur. J. Radiol. 70*, 393−400.

(17) Beosen, M., Østergaard, M., Cimmino, M. A., Kubassova, O., Jensen, K. E., and Bliddal, H. (2009) MRI quantification of rheumatoid arthritis: Current knowledge and future perspectives. *Eur. J. Radiol. 71*, 189−96.

(18) Ramani, A., Jensen, J. H., and Helpern, J. A. (2006) Quantitative MR imaging in Alzheimer disease. *Radiology 241*, 26−44.

(19) Seppi, K., and Schocke, M. F. (2005) An update on conventional and advanced magnetic resonance imaging techniques in the differential diagnosis of neurodegenerative parkinsonism. *Curr. Opin. Neurobiol. 18*, 370−5.

(20) Jinnan, W., Niranjan, B., Gador, C., and Chun, Y. (2010) Imaging biomarkers of cardiovascular disease. *J. Magn. Reson. 32*, 502−15.

(21) Weckbach, S., and Schoenberg, S. O. (2009) Whole body MR imaging in diabetes. *Eur. J. Radiol. 70*, 424−30.

(22) Weckbach, S. (2009) Whole-body MR imaging for patients with rheumatism. *Eur. J. Radiol. 70*, 431−41.

(23) Cryer, B., and Feldman, M. (1998) Cyclooxygenase-1 and cyclooxygenase-2 selectivity of widely used nonsteroidal anti-inflammatory drugs. *Am. J. Med. 104*, 413−21.

(24) Chrysanthakopoulos, M., Giaginis, C., and Tsantili-Kakoulidou, A. (2010) Retention of structurally diverse drugs in human serum albumin chromatography and its potential to simulate plasma protein binding. *J. Chromatogr. A 1217*, 5761−8.

(25) DrugBank Open Data Drug & Drug Target Database, http://www.drugbank.ca/ (accessed Apr 2014).

(26) Thompson, M. K., Misselwitz, B., Tso, L. S., Doble, D. M. J., Schmitt-Willich, H., and Raymond, K. N. (2005) In vivo evaluation of gadolinium hydroxypyridonate chelates: initial experience as contrast media in magnetic resonance imaging. *J. Med. Chem. 48*, 3874−7.

(27) Mohs, A. M., Zong, Y., Guo, J., Parker, D. L., and Lu, Z.-R. (2005) PEG-*g*-poly(GdDTPA-*co*-L-cystine): effect of PEG chain length on in vivo contrast enhancement in MRI. *Biomacromolecules 6*, 2305−11.

(28) Chan, K. W.-Y., Barra, S., Botta, M., and Wong, W.-T. (2004) Novel gadolinium(III) polyaminocarboxylate macrocyclic complexes as potential magnetic resonance imaging contrast agents. *J. Inorg. Biochem. 98*, 677−82.

(29) Li, C., Li, Y.-X., Law, G.-L., Man, K., Wong, W.-T., and Lei, H. (2006) Fast water-exchange Gd^{3+}-(DO3A-like) complex functionalized with Aza-15-Crown-5 showing prolonged residence lifetime in vivo. *Bioconjugate Chem. 17*, 571−4.

(30) Taniura, S., Kamitani, H., Watanabe, T., and Eling, T. E. (2002) Transcriptional regulation of cyclooxygenase-1 by histone deacetylase inhibitors in normal human astrocyte cells. *J. Biol. Chem. 277*, 16823−30.

(31) Taniura, S., Kamitani, H., Wantanabe, T., and Eling, T. E. (2008) Induction of cyclooxygenase-2 expression by Interleukin-1b in human glioma cell line, U87MG. *Neurologia Medico-Chirurfica (Tokyo) 48*, 500−05.

(32) Crofford, L. J., Wilder, R. L., Ristimaki, A. P., Sano, H., Remmers, E. F., Epps, H. R., and Hla, T. (1994) Cyclooxygenase-1 and −2 Expression in Rheumatoid Synovial Tissues. Effects of Interleukin-1β, Phorbol Ester, and Corticosteroids. *J. Clin. Invest. 93*, 1095−101.

(33) Dadabhoy, A., Faulkner, S., and Sammes, P. G. (2002) Long wavelength sensitizers for europium(III) luminescence based on acridone derivatives. *J. Chem. Soc., Perkin Trans. 2*, 348−57.

(34) Lauffer, R. B. (1987) Paramagnetic metal complexes as water proton relaxation agents for NMR imaging: theory and design. *Chem. Rev. 87*, 901−27.

(35) Powell, D. H., Dhubhghaill, O. M. N., Pubanz, D., Helm, L., Lebedev, Y. S., Schlaepfer, W., and Merbach, A. E. (1996) Structural and dynamic parameters obtained from ^{17}O NMR, EPR, and NMRD studies of monomeric and dimeric Gd^{3+} complexes of interest in magnetic resonance imaging: an integrated and theoreticaly self-consistent approach. *J. Am. Chem. Soc. 118*, 9333−46.

(36) Deepa, S., and Mishra, A. K. (2005) Fluorescence spectroscopic study of serum albumin−bromadiolone interaction: fluorimetric determination of bromadiolone. *J. Pharm. Biomed. Anal. 38*, 556−63.
(37) Wang, Y.-Q., Zhang, H.-M., Zhang, G.-C., Tao, W.-H., and Tang, S.-H. (2007) Interaction of the flavonoid hesperidin with bovine serum albumin: A fluorescence quenching study. *J. Lumin. 126*, 211−8.
(38) Lakowicz, J. R., and Weber, G. (1973) Quenching of fluorescence by oxygen. a probe for structural fluctuations in macromolecules. *Biochemistry 12*, 4161−70.
(39) Wu, S.-S., Yuan, W.-B., Wang, H.-Y., Zhang, Q., Liu, M., and Yu, K.-B. (2008) Synthesis, crystal structure and interaction with DNA and HSA of (N,N′-dibenzylethane-1,2-diamine) transition metal complexes. *J. Inorg. Biochem. 102*, 2026−34.
(40) Zsila, F., Bikadi, Z., Malik, D., Hari, P., Pechan, I., Berces, A., and Hazai, E. (2011) Evaluation of drug-human serum albumin binding interactions with support vector machine aided online automated docking. *Bioinformatics*, 1−8.
(41) Carter, D. C., and Ho, J. X. (1994) *Advances in Protein Chemistry*, pp 153−203, Vol *45*, Academic Press, Inc., New York.
(42) Blatt, E., Ghiggino, K. P., and Sawyer, W. H. (1981) A novel means of investigating the polarity gradient in the micelle sodium lauryl sulphate using a series of n-(9-anthroyloxy) fatty acids as flruorescent probes. *J. Chem. Soc., Faraday Trans. 1 77*, 2551−8.
(43) Hermann, P., Kotek, J., Kubíček, V., and Lukeš, I. (2008) Gadolinium(III) complexes as MRI contrast agents: ligand design and properties of the complexes. *Dalton Trans.*, 3027−47.
(44) Woo, D. H., Han, I.-S., and Jung, G. (2004) Mefenamic acid-induced apoptosis in human liver cancer cell-lines through caspase-3 pathway. *Life Sci. 75*, 2439−49.
(45) Turetschek, K., Floyd, E., Helbich, T., Roberts, T. P. L., Shames, D. M., Wendland, M. F., Carter, W. O., and Brasch, R. C. (2001) MRI assessment of microvascular characteristics in experimental breast tumors using a new blood pool contrast agent (MS-325) with correlations to histopathology. *J. Magn. Reson. Imaging 14*, 237−42.
(46) Adzamli, K., Yablonskiy, D. A., Chicoine, M. R., Won, E. K., Galen, K. P., Zahner, M. C., Woolsey, T. A., and Ackerman, J. J. H. (2003) Albumin-binding MR blood pool agents as MRI contrast agents in an intracranial mouse glioma model. *Magn. Reson. Med. 49*, 586−90.
(47) Jayson, M. I. V., and Dixon, A. S. J. (1970) Intra-articular pressure in rheumatoid arthritis of the knee. *Ann. Rheum. Dis. 29*, 261−5.
(48) Wallis, W. J., Simkin, P. A., and Nelp, W. B. (1987) Protein traffic in human synovial effusions. *Arthritis Rheum. 30*, 57−63.
(49) Levick, J. R. (1981) Permeability of rheumatoid and normal human synovium to specific plasma proteins. *Arthritis Rheum. 24*, 1550−60.
(50) Barge, A., Cravotto, G., Gianolio, E., and Fedeli, F. (2006) How to determine free Gd and free ligand in solution of Gd chelates. A technical note. *Contrast Media Mol. Imaging 1*, 184−8.
(51) Lo, K. K.-W., Chung, C.-K., and Zhu, N. (2006) Nucleic acid intercalators and avidin probes derived from luminescent cyclometalated iridium(III)-dipyridoquinoxaline and -dipyridophenazine complexes. *Chem.—Eur. J. 12*, 1500−12.
(52) Lo, K. K.-W., and Leung, A. H.-H. (2010) Luminescent cyclometalated iridium(III) dipyridoquinoxaline indole complexes as biological probes. *Sci. China Chem. 53*, 2091−8.
(53) Harte, A. J., and Gunnlaugsson, T. (2006) Synthesis of α-chloroamides in water. *Tetrahedron Lett. 47*, 6321−4.
(54) Dimiza, F., Papadopoulos, A. N., Tangoulis, V., Psycharis, V., Raptopoulou, C. P., Kessissoglou, D. P., and Psomas, G. (2010) Biological evaluation of non-steroidal anti-inflammatory drugs-cobalt-(II) complexes. *Dalton Trans. 39*, 4517−28.
(55) Kalber, T. L., Kamaly, N., Higham, S. A., Pugh, J. A., Bunch, J., McLeod, C. W., Miller, A. D., and Bell, J. D. (2011) Synthesis and characterization of a theranostic vascular disrupting agent for in vivo MR imaging. *Bioconjugate Chem. 22*, 879−86.